7

Fatigue Behaviour of Welded Joints Made of 6061-T651 Aluminium Alloy

Alfredo S. Ribeiro and Abílio M.P. de Jesus
UCVE, IDMEC-Pólo FEUP
School of Sciences and Technology, University of Trás-os-Montes and Alto Douro
Portugal

1. Introduction

The purpose of this chapter is to present the main results of an investigation concerning the assessment of the fatigue behaviour of welded joints made of the 6061-T651 aluminium alloy. The 6061 aluminium alloy is one of the most common aluminium alloys for heavy-duty structures requiring good corrosion resistance, truck and marine components, railroad cars, furniture, tank fittings, general structures, high pressure applications, wire products and pipelines. Many of these applications involves variable loading, which makes very relevant the study of the fatigue behaviour of this aluminium allow. In particular, the study of the fatigue behaviour of welded joints is of primordial importance since welds are intensively used for structural applications. The proposed investigation focuses in four types of welded joints, made from 12 mm thick aluminium plates, namely one butt welded joint and three types of fillet joints: T-fillet joint without load transfer, a load-carrying fillet cruciform joint and a longitudinal stiffener fillet joint.

Traditionally, the fatigue assessment of welded joints, including those made of aluminium alloys, is based on the so-called S-N approach (Maddox, 1991). This approach, which is included in main structural design codes of practice, adopts a classification system for details, and proposes for each fatigue class an experimental-based S-N curve, which relates the applied stress range (e.g. nominal, structural, geometric) with the total fatigue life. Alternatively to this S-N approach, the Fracture Mechanics has been proposed to assess the fatigue life of the welded joints. It is very often claimed that welded joints have inherent crack-like defects introduced by the welding process itself. Therefore, the fatigue life of the welded joints may be regarded as a propagation process of those defects. A relation between the Fracture Mechanics and the S-N approaches is usually assumed. The slope of the S-N curves is generally understood to be equal to the exponent of the power relation governing the fatigue crack propagation rates of fatigue cracks.

More recently, the local approaches to fatigue have gaining added interest in the analysis of welded joints (Radaj et al., 2009). In general, such approaches are based on a local damage definition (e.g. notch stresses or strains) which makes these approaches more adequate to model local damage such as the fatigue crack initiation. In this sense, the Fracture Mechanics can be used to complement the local approaches, since the first allows the computation of the number of cycles to propagate an initial crack until final failure of the component.

The present research seeks to understand the significance of the fatigue crack initiation, evaluated using a local strain-life approach, on the total fatigue life estimation for four types

of welded joints made of 6061-T651 aluminium alloy. The Fracture Mechanics is also applied to assess the fatigue crack propagation, in order to allow a comparison with the crack initiation predictions and also with the global S-N data, made available for the welded joints by means of constant amplitude fatigue tests.
In the section 2 of the chapter, the 6061-T651 aluminium alloy is described. Then, on section 3 the basic fatigue properties of the material are presented. The strain-life fatigue data as well as the fatigue crack propagation data of the 6061-T651 aluminium alloy (base material) are presented. Also, the fatigue crack propagation data is presented for the welded and heat affected materials. On section 4, the fatigue S-N data obtained for the welded details is presented. Section 5 is devoted to the fatigue modelling of the welded details. Finally, on section 6, the conclusions of the research are presented.

2. The 6061-T651 aluminium alloy

This research was conducted on an AlMgSi aluminium alloy: the 6061-T651 aluminium alloy. The 6061-T651 alloy is a precipitation hardening aluminium alloy, containing Magnesium and Silicon as its major alloying elements. The T651 treatment corresponds to stress-relieved stretch and artificially aging. The typical chemical composition of the 6061-T651 aluminium alloy is shown in Table 1. The high Magnesium content is responsible for the high corrosion resistance and good weldability. The proportions of Magnesium and Silicon available are favourable to the formation of Magnesium Silicide (Mg_2Si). The material used in this research was delivered in the form of 12 mm and 24 mm thick plates. This alloy is perhaps one of the most versatile of heat treatable aluminium alloys. It has good mechanical properties. It is one of the most common aluminium alloys for general purpose applications. It was developed for applications involving moderate strength, good

Si	**Fe**	**Cu**	**Mn**	**Mg**	**Cr**
0.69	0.29	0.297	0.113	0.94	0.248
Zn	**Ti**	**B**	**Zr**	**Pb**	**Ti+Zr**
0.15	0.019	0.0021	0.001	0.02	0.02

Table 1. Chemical composition of the 6061-T651 aluminium alloy (weight %)

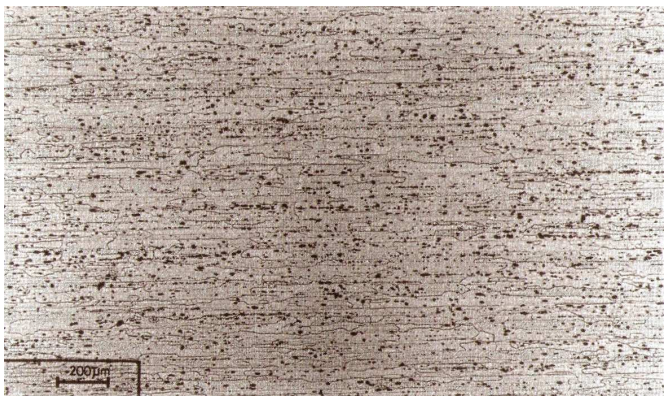

Fig. 1. Microstructure of the 6061-T651 aluminium alloy according the rolling direction

formability and weldability. Because of such desirable properties, this alloy is used in civilian and militaries industries. Figure 1 illustrates a typical microstructure of the aluminium alloy evaluated along the rolling or longitudinal direction. It is visible the stretched grains due to the rolling process. Also, a dispersed second phase typical of deformed and heat treated wrought aluminium alloys is observed.

3. Fatigue behaviour of the 6061-T651 aluminium alloy

3.1 Strain-life fatigue relations

Strain-life fatigue results, derived using smooth specimens, are usually applied to model the macroscopic fatigue crack initiation. An initiation criteria based on a 0.25 mm depth crack is commonly used by some authors (De Jesus, 2004). One important strain-life relation was proposed by Coffin (1954) and Manson (1954), which relates the plastic strain amplitude, $\Delta\varepsilon_p/2$, with the number of reversals to crack initiation, $2N_f$:

$$\frac{\Delta\varepsilon_p}{2} = \varepsilon'_f (2N_f)^c \tag{1}$$

where ε'_f and c are, respectively, the fatigue ductility coefficient and fatigue ductility exponent. The Coffin-Manson relation, which is valid for low-cycle fatigue, can be extended to high-cycle fatigue domains using the relation proposed by Basquin (1910). The latter relates the elastic strain amplitude, $\Delta\varepsilon_e/2$, with the number of reversals to failure, $2N_f$:

$$\frac{\Delta\varepsilon_e}{2} = \frac{\sigma'_f}{E}(2N_f)^b \tag{2}$$

where σ'_f is the fatigue strength coefficient, b is the fatigue strength exponent and E is the Young's modulus. The number of reversals corresponding to the transition between low- and high-cycle fatigue regimes is characterised by total strain amplitude composed by equal components of elastic and plastic strain amplitudes. Lives below this transition value are dictated by ductility properties; lives above this transition value are dictated by strength properties. Morrow (1965) suggested the superposition of Equations (1) and (2), resulting in a more general equation, valid for low- and high-cycle fatigue regimes:

$$\frac{\Delta\varepsilon}{2} = \frac{\Delta\varepsilon_e}{2} + \frac{\Delta\varepsilon_p}{2} = \frac{\sigma'_f}{E}(2N_f)^b + \varepsilon'_f (2N_f)^c \tag{3}$$

Equation (3) may be changed to account for mean stress effects, resulting:

$$\frac{\Delta\varepsilon}{2} = \frac{\sigma'_f - \sigma_m}{E}(2N_f)^b + \varepsilon'_f (2N_f)^c \tag{4}$$

where σ_m stands for the mean stress. The application of Equations (3) and (4) requires the knowledge of the stabilized strain amplitude, $\Delta\varepsilon/2$, at the point of interest of the structure. The computation of the strain amplitude requires the prior knowledge of the cyclic curve of the material, which relates the stabilized strain and stress amplitudes. The cyclic curve is usually represented using the Ramberg-Osgood relation (Ramberg & Osgood, 1943):

$$\frac{\Delta\varepsilon}{2}=\frac{\Delta\sigma}{2E}+\left(\frac{\Delta\sigma}{2k'}\right)^{1/n'} \tag{5}$$

where k' is the cyclic hardening coefficient and n' is the cyclic hardening exponent. Equation (5) may also be used to describe the hysteresis loops branches if the material shows Masing behaviour. In these cases, the hysteresis loops results from the magnification of the cyclic stress-strain curve by a scale factor of two.

3.2 Experimental strain-life data

Eight smooth specimens were tested under strain controlled conditions in order to identify the strain-life and cyclic elastoplastic behaviour of the 6061-T651 aluminium alloy. The geometry and dimensions of the specimens are represented in Figure 2 and are in agreement with the recommendations of ASTM E606 (ASTM, 1998). After machining, the specimen surfaces were mechanically polished. The experiments were carried out in a close-loop servohydraulic test machine, with 100 kN load capacity. A sinusoidal waveform was used as command signal. The fatigue tests were conducted with constant strain amplitudes, at room temperature, in air. The longitudinal strain was measured using a longitudinal extensometer with a base length equal to 12.5 mm and limit displacements of ±2.5 mm. The specimens were cyclic loaded under strain control with symmetrical push-pull loading, with a nominal strain ratio, $R_\varepsilon=-1$. The nominal strain rate $d\varepsilon / dt$ was kept constant in all specimens at the value $8\times10^{-3}s^{-1}$ in order to avoid any influence of the strain rate on the hysteresis loop shape. The cyclic stress-strain curves were determined using the method of one specimen for each imposed strain level. The stable hysteresis loop was defined as the hysteresis loop for 50% of the fatigue life. The specimens were tested with imposed strain ranges between 0.9% and 3.5%. The monotonic stress-strain curves were also experimentally determined for comparison purposes.

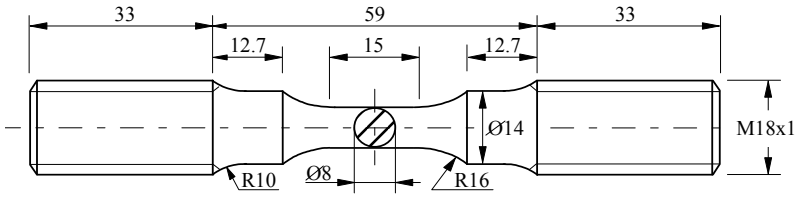

Fig. 2. Geometry and dimensions of the specimens used in the strain-controlled fatigue tests (dimensions in mm)

The monotonic strength and elastic properties of the 6061-T651 aluminium alloy are presented in Table 2. Table 2 also includes the properties obtained by Moreira et al. (2008), for the 6061-T6 aluminium alloy, and by Borrego et al. (2004), for the 6082-T6 aluminium alloy, for comparison purposes. In general, the three materials show comparable properties. However, a detailed comparison reveals that the 6082-T6 alloy presents better monotonic strength with slightly lower ductility than the 6061-T651 aluminium alloy. This may be due to the fact that the 6082 aluminium alloy exhibits higher Silicon (1.05) and Manganese contents (0.68) than the 6061 aluminium alloy (Ribeiro et al., 2009). The 6061-T6 aluminium alloy shows slightly higher strength properties and very similar ductility properties than the

6061-T651 aluminium alloy. The T6 treatment does not include any stress relieve by stretch as performed by the T651 treatment.

Properties	6061-T651	6061-T6	6082-T6
Tensile strength, σ_{UTS} (MPa)	290-317	310-342	330
Yield strength, $\sigma_{0.2\%}$ (MPa)	242-279	276-306.3	307
Elongation, ε_r (%)	10.0-15.8	12.0-17.1	9
Young modulus, E (GPa)	68.0	68.5-68.9	70

Table 2. Monotonic strength and elastic properties of the 6061-T651, 6061-T6 and 6082-T6 aluminium alloys

Figure 3 shows the cyclic behaviour of the 6061-T651 aluminium alloy, namely the stabilized stress amplitude is plotted against the corresponding strain amplitude. The 6061-T651 aluminium alloy, despite not presenting a significant cyclic hardening, it shows some hardening for strain amplitudes above 1%. Cyclic softening is verified for strain amplitudes bellow 1.0%. Figure 4 compares the cyclic and monotonic curves of the material, which further validates the previous observations. Figure 5 plots the stabilized stress amplitude against the plastic strain amplitude. It is verified that both parameters follows a power relation as described by the non-linear term of the Ramberg-Osgood relation (Equation (5)). Figure 6 presents the total strain amplitude versus life curve obtained from the superposition of the elastic and plastic strain amplitude versus life curves. The number of reversals of transition, $2N_T$, verified for 6061-T651 aluminium alloy was 969 reversals. The

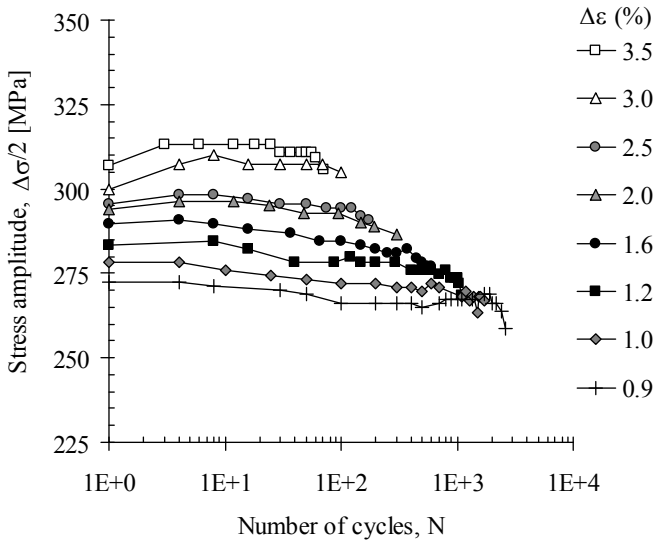

Fig. 3. Stress amplitude versus number of cycles from fully-reversed strain-controlled tests obtained for the 6061-T651 aluminium alloy

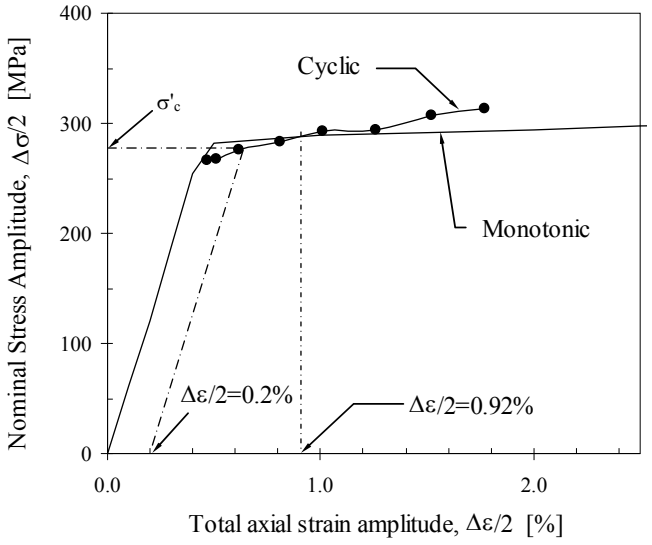

Fig. 4. Comparison of monotonic and cyclic stress-strain curves of the 6061-T651 aluminium alloy

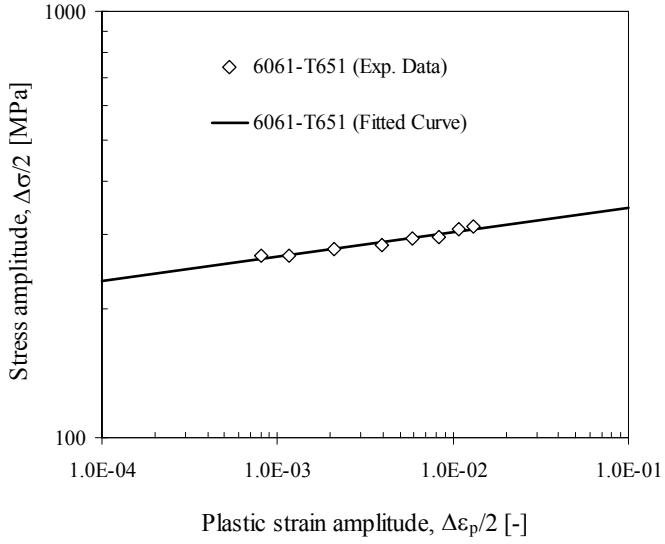

Fig. 5. Cyclic curve of the 6061-T651 aluminium alloy

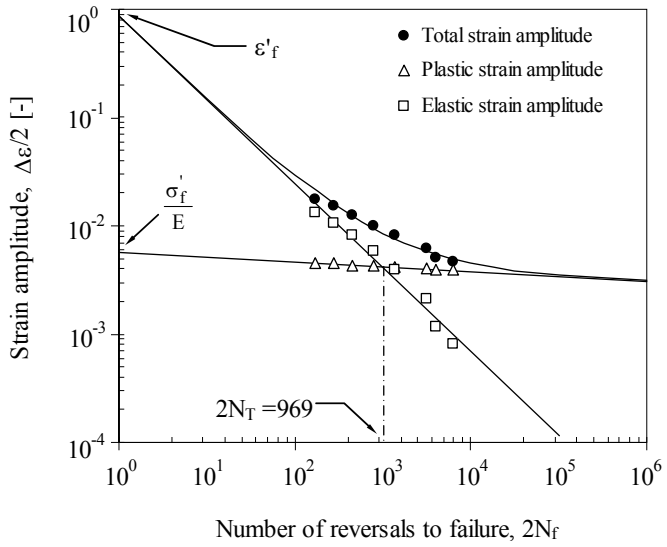

Fig. 6. Strain-life data of the 6061-T651 aluminium alloy

Properties	6061-T651	6061-T6	6082-T6
Fatigue strength coefficient, σ'_f [MPa]	394	383	487
Fatigue strength exponent, b	-0.045	-0.053	-0.07
Fatigue ductility coefficient, ε'_f (-)	0.634	0.207	0.209
Fatigue ductility exponent, c	-0.723	-0.628	-0.593
Cyclic strain hardening coef., k' [MPa]	404	-	444
Cyclic strain hardening exponent, n'	0.062	0.089	0.064

Table 3. Strain-life and cyclic properties of the 6061-T651, 6061-T6 and 6082-T6 aluminium alloys

fatigue ductility and strength properties of the alloy were derived from results shown in Figure 6. Table 3 summarizes the fatigue properties of the 6061-T651 aluminium alloy as well as the cyclic elastoplastic constants. Also, the properties obtained by Borrego et al. (2004), for the 6062-T6 aluminium alloy, and Chung & Abel (1988), for the 6061-T6 aluminium alloy, are included for comparison purposes. The 6061-T651 aluminium alloy shows significantly higher fatigue ductility than the other aluminium alloys.

3.3 Fatigue crack propagation relations

The evaluation of the fatigue crack propagation rates has been a subject of intense research. The Linear Elastic Fracture Mechanics (LEFM) has been the most appropriate methodology to describe the propagation of fatigue cracks. The LEFM is based on the hypothesis that the

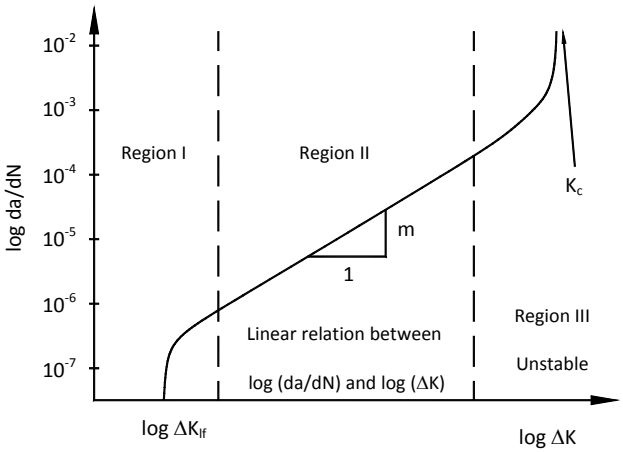

Fig. 7. Schematic representation of the relation between da / dN and ΔK

stress intensity factor is the mechanical parameter that controls the stress range at the crack tip. The typical fatigue crack propagation data is presented in the form of fatigue crack propagation rates versus stress intensity factor range diagrams. A typical diagram is illustrated in Figure 7. The da / dN versus ΔK curves are usually derived, for the majority of high strength materials, for crack propagation rates ranging between 10^{-7} and 10^{-2} mm/cycle. The diagram illustrates three different propagation regions, usually designated by regions I, II and III. In the region I, the propagation rate depends essentially on the stress intensity factor. In this region there exists a ΔK value below which no propagation is verified, or if propagation exists the propagation rate is below 10^{-7} mm/cycle. This value of the stress intensity factor range is denominated propagation threshold and it is represented by ΔK_{If} . In the region II, a linear relation between $\log(da / dN)$ and $\log(\Delta K)$ is observed. Region III appears when the maximum value of the stress intensity factor approaches the fracture toughness of the material, K_{Ic} or K_c . This region is characterized by an acceleration of the crack propagation rate that leads to an unstable propagation of the crack and consequently to the final rupture. The region III is not well defined for materials experiencing excessive ductility. For these materials the development of gross plastic deformations is observed in region III which invalidates the application of the LEFM, since the basic hypothesis of the LEFM are violated.

A great number of fatigue crack propagation laws have been proposed in literature, however the most used and simple relation was proposed by Paris & Erdogan (1963):

$$\frac{da}{dN} = C\Delta K^m \tag{6}$$

where da / dN is the fatigue crack propagation rate, $\Delta K = K_{\max} - K_{\min}$ represents the range of the stress intensity factor and C and m are materials constants. This relation describes the region II of fatigue crack propagation. The number of cycles to propagate a crack from an initial size, a_i , to a final size, a_f , may be computed integrating the fatigue crack propagation law. In the case of the Paris's law, this integration may be written in the following form:

$$N = \frac{1}{C}\int_{a_i}^{a_f} \frac{da}{\Delta K^m} = \frac{1}{C}\frac{1}{\Delta\sigma^m}\int_{a_i}^{a_f} \frac{da}{\left(Y\sqrt{\pi a}\right)^m} \tag{7}$$

Equation (7) may be used to compute the number of cycles to failure if a_f corresponds to the critical crack size, leading to failure.

3.4 Fatigue crack propagation data

In order to determine the fatigue crack propagation curves, Compact Tension (CT) specimens were used. This specimen geometry presents, in relation to the alternative Centre Crack Tension geometry (CCT), the advantage of providing a larger number of readings with a smaller material volume requirement. The specimens were cut from a 24 mm thick plate of 6061-T651 aluminium alloy, containing a butt welded joint made from both sides using the MIG welding process. The filler material used in the welding process was the AlMg-5356. Due to material limitations, specimens with thickness B=10 mm and nominal width W=50 mm were used. These dimensions are according to the recommendations of the ASTM E647 standard (ASTM, 2000). Figure 8 illustrates the locations in the aluminium plate from where the specimens were extracted. Specimens containing base material (BM), heat affected zone (HAZ) and welded material (WEL) were cut from the plate. This extraction process was planned in agreement with the recommendations included in the standard. The specimens were tested in a servohydraulic machine, rated to 100 kN, applying a sinusoidal waveform with 15 Hz. The crack length was measured on both faces of the specimen, using two magnifying eyeglasses. The resolution of the measuring device was 0.01 mm.

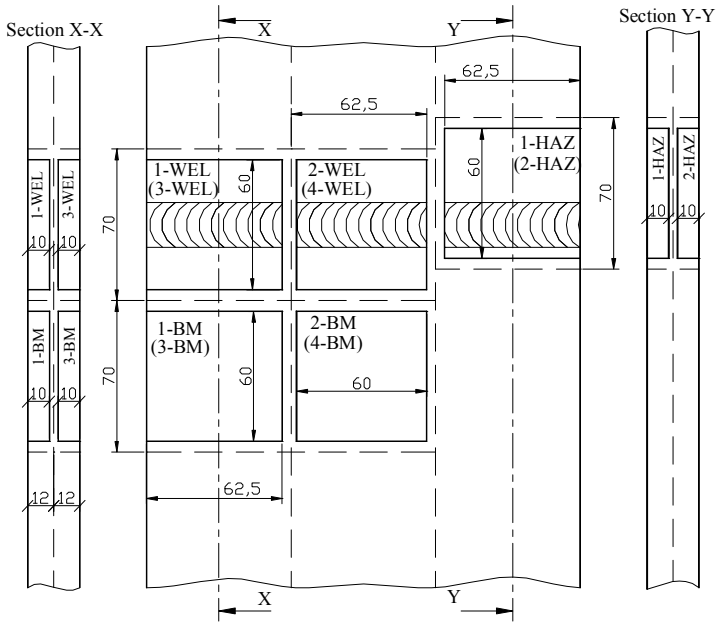

Fig. 8. Locations of the CT specimens at the welded plate (dimensions in mm)

In order to obtain the da/dN versus ΔK curves it is necessary to find an appropriate expression to evaluate ΔK. The ASTM E647 standard (ASTM, 2000) proposes the following formulation of ΔK, for the CT geometry:

$$\Delta K = \Delta\sigma \cdot f\left(\frac{a}{W}\right) \tag{8}$$

where $f(a/W)$ is the compliance function that is specified in the standard and $\Delta\sigma$ is the applied stress range. For the CT geometry $\Delta\sigma$ assumes the following form:

$$\Delta\sigma = \frac{\Delta P}{B \cdot W^{1/2}} \tag{9}$$

where ΔP is the applied load range, B and W define, respectively, the thickness and the nominal width of the specimen.

Table 4 summarizes the experimental program carried out in order to derive the da/dN versus ΔK for the base material, heat affected zone, and welded material. The stress ratios tested were R=0.1 and R=0.5. The frequency of the tests, f, was 15 Hz. The table also includes the maximum and minimum loads of the test. It was verified that for some tests, namely for tests performed with welded material, the crack deviates from the ideal shape, namely a divergence between the crack on the two faces of the specimen was verified. This phenomenon can be explained by the following factors: misalignments, asymmetrical disposition of the welding or existence of inclusions, oxides or porosities in the welding.

Specimen	**Material**	***R***	***f*** **[Hz]**	F_{max} **[N]**	F_{min} **[N]**
2 - BM	Material Base	0.1	15	3676.8	367.6
3 - BM		0.5	15	8372.7	4186.3
1 - WEL	Welded Material	0.1	15	3231.0	323.1
3 - WEL		0.1	15	3600.0	360.0
2 - WEL		0.5	15	6205.5	3102.7
1 - HAZ	HAZ	0.1	15	29652	296.52
2 - HAZ		0.5	15	4688.2	2344.1

Table 4. Crack propagation experimental program

The evaluation of the fatigue crack propagation rates was made through the seven point polynomial incremental method as proposed in the ASTM E647 standard (ASTM, 2000). Figures 9 to 11 represent the da/dN versus ΔK curves for the base material, welded material and heat affected zone and for stress ratios R=0.1 and R=0.5. The results correspond to the region II, region of validity of the Paris's law. Figures 12 and 13 compare the propagation curves for the three tested materials, respectively for R=0.1 and R=0.5. It can be concluded that the propagation rates increase with the increase of R. This influence is more significant for low values of ΔK. R influences the crack propagation curves for the three materials but its influence is more significant for the base material. The HAZ shows low sensitivity to the stress ratio. It can be observed that HAZ presents the greatest propagation

rates for R=0.1. The propagation rates of the welded material present intermediate values between HAZ and the base material. Tests conducted with R=0.5 do not show significant differences in the propagation rates for the three materials. The factors that justify these results are several, such as the elevated levels of residual stresses at the crack tip, the effect of the stress ratio, the yield stress and the grain size that is distinct for the three materials. The parameters of the Paris's law are listed in the Table 5 for the three materials and for the two stress ratios, R=0.1 and R=0.5. The determination coefficients, R^2, obtained for the adjusted curves are significant.

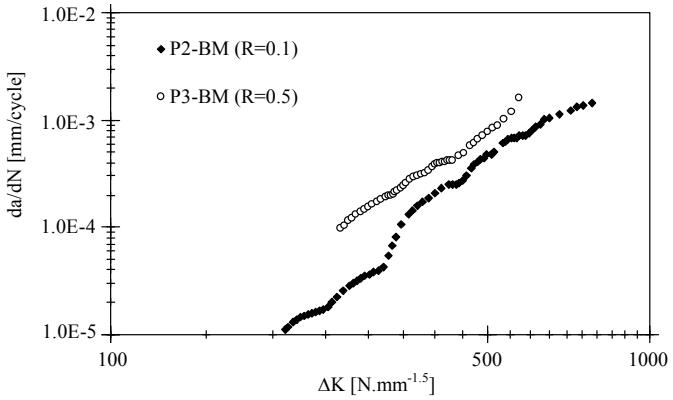

Fig. 9. Fatigue crack propagation rates for the base material

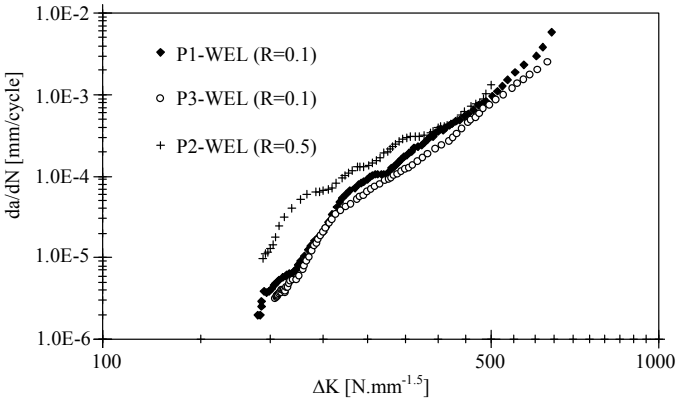

Fig. 10. Fatigue crack propagation rates for the welded material

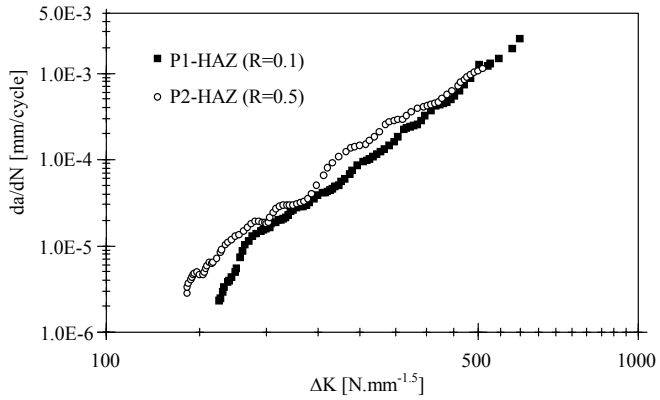

Fig. 11. Fatigue crack propagation rates for the heat affected material

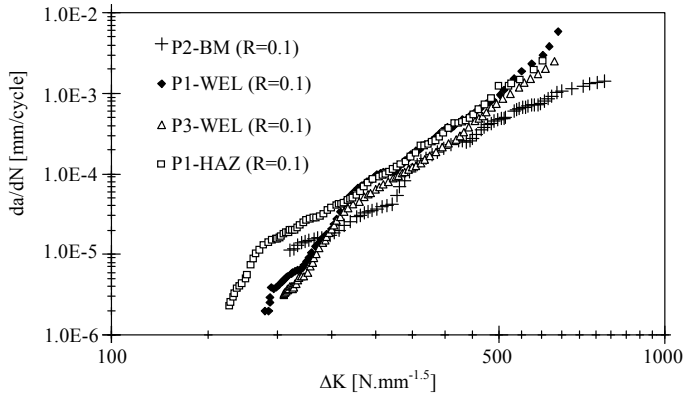

Fig. 12. Comparison of fatigue crack propagation rates for R=0.1

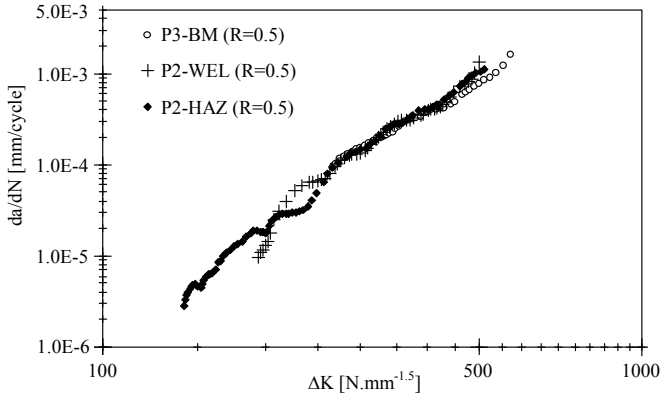

Fig. 13. Comparison of fatigue crack propagation rates for R=0.5

Material	R	$da/dN = C\Delta K^m$			R^2
		C^*	C^{**}	m	
BM	0.1	1.9199E-15	3.7086E-12	4.1908	0.9822
BM	0.5	1.2863E-12	9.8151E-11	3.2547	0.9912
WEL	0.1	6.5017E-20	6.7761E-14	6.0120	0.9731
WEL	0.5	1.9094E-15	6.7566E-12	4.3657	0.9639
HAZ	0.1	1.1363E-16	1.7580E-12	4.7932	0.9863
HAZ	0.5	8.7433E-16	4.8669E-12	4.4972	0.9930
BM	0.1;0.5	1.3790E-14	1.0619E-11	3.9242	0.8592
WEL	0.1;0.5	4.5939E-19	1.6769E-13	5.7082	0.9249
HAZ	0.1;0.5	5.4406E-16	3.6208E-12	4.5489	0.9770
BM; WEL; HAZ	0.1	3.2668E-17	8.3120E-13	4.9371	0.9314
BM; WEL; HAZ	0.5	2.0587E-15	6.7596E-12	4.3444	0.9835
BM; WEL; HAZ	0.1; 0.5	2.6567E-16	2.2733E-12	4.6217	0.9039

*da/dN (mm/cycle) and ΔK (N.mm-1.5)
**da/dN (m/cycle) and ΔK (MPa.m0.5)

Table 5. Constants of Paris's law of the tested materials

4. Fatigue behaviour of welded joints made of 6061-T651 aluminium alloy

The proposed investigation focused in four types of welded joints, made from 12 mm thick aluminium plates of 6061-T651 aluminium alloy, namely one butt welded joint and three types of fillet joints (see Figure 14). As described in Figure 14, detail 1 corresponds to a butt welded joint; detail 2 corresponds to a T-fillet joint without load transfer; detail 3 corresponds to a load-carrying fillet cruciform joint and finally, detail 4 is a longitudinal stiffener fillet joint. Welds were performed with the manual MIG process with Al Mg-5356 filler material (ϕ1.6 mm) and Argon + 0.0275% NO gas protection (17 litres/min). The butt welded joint was prepared with a V-chamfer. For the fillet welds, no chamfer was required. The butt welded joint was made using two weld passes; each fillet of the fillet joints was made using a single weld pass. Details 1 to 3 were subjected to a pos-welding alignment using a 4-Point bending system. No stress relieve was used after the alignment procedure. Detail 4 was tested in as-welded condition.

For each type of geometry, a test series was prepared and tested under constant amplitude fatigue loading conditions, in order to derive the respective S-N curves. The tests were carried out on a MTS servohydraulic machine, rated to 250 kN. Remote load control was adopted in the fatigue tests, under a sinusoidal waveform. A load ratio equal to 0.1 was adopted. Figure 15 represents the experimental S-N data obtained for each welded detail, using the nominal/remote stress range as a damage parameter. Small corrections were introduced into the theoretical remote stress range, using the information from strain measurements carried out on a sample of specimens.

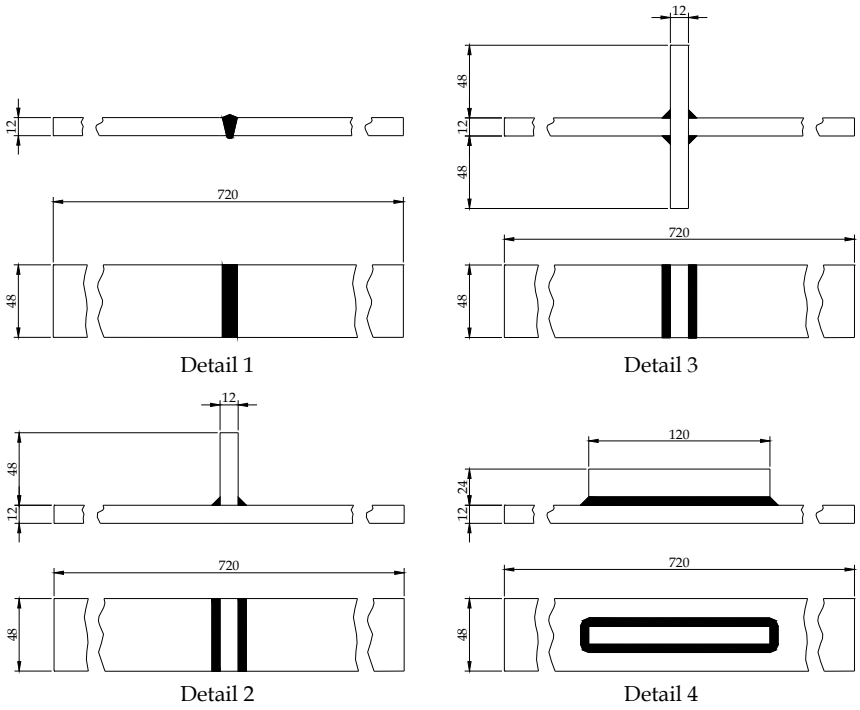

Fig. 14. Welded joints made of 6061-T651 aluminium alloy (dimensions in mm)

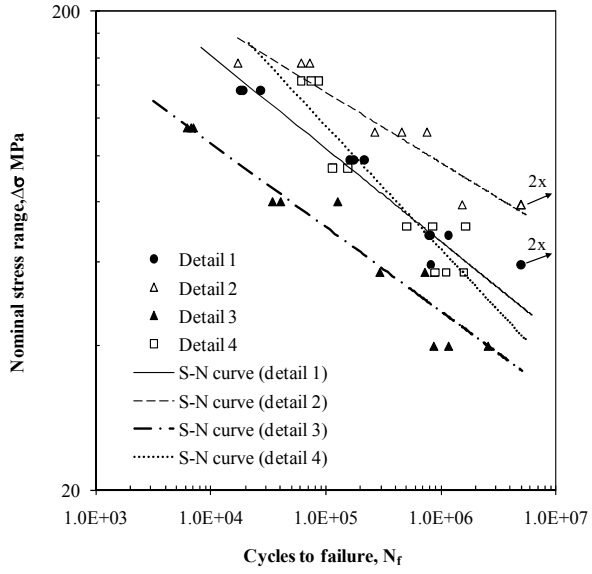

Fig. 15. S-N fatigue data from the welded specimens

The usual way to express the S-N fatigue data is to use a power relation that is often expressed in one of the following ways:

$$\Delta\sigma^{m} N_f = C \tag{10}$$

$$\Delta\sigma = A N_f^{\alpha} \tag{11}$$

where m, C, A and α are constants. Table 6 summarizes the constants for each test series obtained using linear regression analysis. The determination coefficients are also included in the table. Relative high determination coefficients are observed. S-N curves derived for the details 1 to 3 are rather parallel. The detail 4 shows a significantly distinct slope. The detail 2 shows the highest fatigue resistance; conversely, detail 3 – the load-carrying T-fillet cruciform joint- shows the lowest fatigue resistance.

Welded details	S-N parameters				R^2
	A	α	C	m	
1	969.530	-0.194	2.305E+15	5.144	0.953
2	739.863	-0.147	2.913E+19	6.784	0.844
3	535.373	-0.176	3.371E+15	5.691	0.926
4	2216.671	-0.257	1.054e+13	3.892	0.848

Table 6. Parameters of the S-N data of the welded details

5. Fatigue modelling of welded joints

5.1 Description of the model

The fatigue life of a structural component can be assumed as a contribution of two complementary fatigue processes, namely the crack initiation and the macroscopic crack propagation, as:

$$N_f = N_i + N_p \tag{12}$$

where N_f is the total fatigue life, N_i is the number of cycles to initiate a macroscopic crack, and N_p is the number of cycles to propagate the crack until final failure. Generally, is it assumed that the fatigue behaviour of welds is governed by a crack propagation fatigue process, since the welding process may introduce initial defects. The validity of this assumption is analysed in this study for four types of welded joints made of 6061-T651 aluminium alloy. Both crack initiation and crack propagation phases are computed and compared with the experimental available S-N data.

The computation of the crack initiation phase will be carried out using the local approaches to fatigue based on the strain-life relations, such as the Morrow's equation (see Equations (3) and (4)). The number of cycles required to propagate the crack will be computed using the LEFM approach, based on Paris's equation (refer to Equations (6) and (7)). The material properties required to perform the referred computations were already presented in the previous sections.

The application of the strain-life relations to compute the crack initiation requires the elastoplastic strain amplitudes at the critical locations, namely at the potential sites for crack initiation. These locations are characterized by a high stress concentration factor, corresponding many times to the notch roots (e.g. weld toes). The elastoplastic strain amplitudes may be calculated using the Neuber's approach (Neuber, 1961):

$$\Delta\sigma \cdot \Delta\varepsilon = k_t^2 \Delta\sigma_{nom} \cdot \Delta\varepsilon_{nom} \tag{13}$$

where $\Delta\sigma$ and $\Delta\varepsilon$ are the total local elastoplastic stress and strain ranges, $\Delta\sigma_{nom}$ and $\Delta\varepsilon_{nom}$ are the nominal stress and strain ranges and k_t is the elastic stress concentration factor. Equation (13) can be used together with the Ramberg-Osgood equation (Equation (5)). Since Equation (13) stands for cyclic loading, some authors replace the elastic stress concentration factor by the fatigue reduction factor, k_f. However, the elastic concentration factor is an upper bound of the fatigue reduction factor. Therefore, in this research, the following conservative assumption is made:

$$k_f = k_t \tag{14}$$

The elastic stress concentration factors for the welded details may be computed based on numerical methods (e.g. FEM), experimental or analytical methods. Ribeiro (1993, 2001) suggested for the welded joints under investigation the elastic stress concentration factors listed in Table 7, based on both finite element analysis and available analytical formulae. The stress concentration factors characterize the stress intensification at the weld toes for details 1, 2 and 4; for detail 3, k_t characterizes the stress intensification at the weld root. Figure 16 shows the potential cracking sites for the investigated details, confirmed by the experimental program.

Welded details	Elastic stress concentration factor, k_t
1	3.50
2	2.60
3	7.24
4	4.43

Table 7. Elastic stress concentration factors

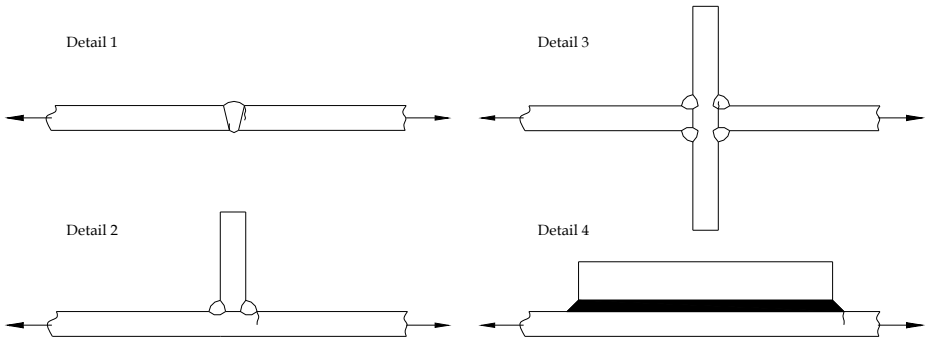

Fig. 16. Potential cracking locations at the investigated welded details

In what concerns the simulation of the fatigue crack propagation, initial defects of 0.25 mm were assumed corresponding to the initiation period. Cracks propagating from the weld toes, perpendicularly to the loading, are assumed for details 1, 2 and 4. For detail 3, a crack propagating from the weld root, perpendicularly to the loading, is assumed (see Figure 16). Constant depth cracks were assumed for details 1 and 3. For details 2 and 4 semi-elliptical cracks were assumed to propagate from the weld toes. In these latter cases, an initial circular crack with a radius equal to 0.25 mm was assumed and Equations (6) and (7) have to be applied twice, namely at both semi-axis endpoints. However, the crack increments are dependent to each other, in order to guarantee the compatibility in the number of propagation cycles, resulting:

$$\frac{da}{dc} = \left(\frac{\Delta K_a}{\Delta K_c} \right)^m \tag{15}$$

where da is the crack increment at the plate surface, dc is the crack increment at the deepest point of the crack front, ΔK_a and ΔK_c are, respectively, the stress intensity factor ranges at the surface and deepest crack front points and m is the Paris's law parameter. The integration of the Paris's law may be easily carried out assuming discrete increments of the crack, for which the stress intensity factors are assumed constant. In order to integrate the Paris's law, the formulations of the stress intensity factors are required. Solutions available in the literature were adopted in this study (Snijder & Dijkstra, 1989). The crack was propagated until it reached 11.8 mm depth (any detail) or 48 mm width for details 2 and 4. Finally, the crack propagation properties presented in section 3.4 were used to simulate the crack propagation period for the welded details. In particular, the properties for R=0.1 were used. For details 1 and 3 the crack propagation data obtained for the welded material was used; for details 2 and 4 the properties obtained for the heat affected material were applied.

5.2 Fatigue predictions

Figures 17 to 20 present the predictions of the fatigue lives for the investigated welded details, made of 6061-T651 aluminium alloy, taking into account the crack initiation and crack propagation phases. Three S-N curves are represented, one corresponding to the fatigue crack initiation, the other corresponding to the fatigue crack propagation and finally the third corresponding to the total fatigue life. Also, the experimental data is included in the graphs for comparison purposes. The analysis of the results reveals that there is a close relation between the fatigue strength and the elastic stress concentration factor. The welded details with higher fatigue resistance show lower elastic stress concentration factors at the critical locations of the welds. The global predictions are in good agreement with the experimental results.

The comparison of the crack initiation based S-N curves with the average experimental data, allows the following comments:

- Crack initiation if significant for butt welded joints, representing about 37% of the total fatigue life for stress ranges equal of higher than 98 MPa.
- For the T-fillet joint without load transfer, the crack initiation is significant representing about 50% of the total fatigue life, for the stress range of 156 MPa. For stress ranges bellow 79 MPa, the crack initiation was about 5×10^6 cycles.

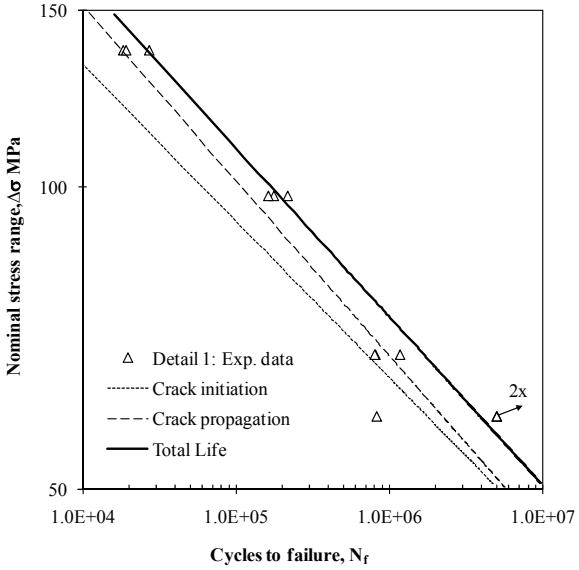

Fig. 17. Fatigue life predictions for the butt welded joint: detail 1

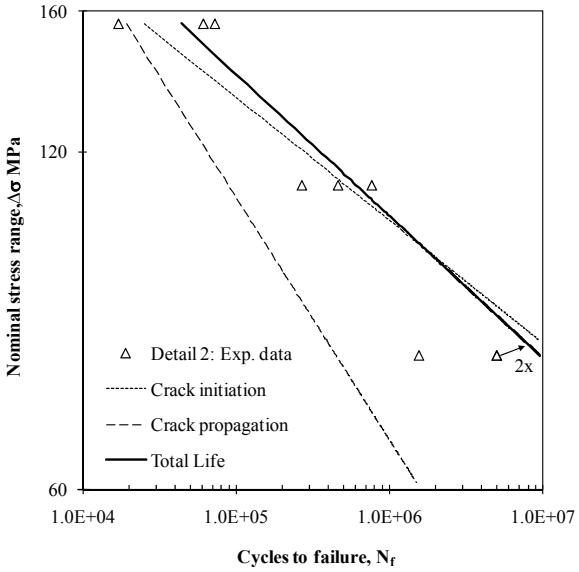

Fig. 18. Fatigue life predictions for the T-fillet joint without load transfer: detail 2

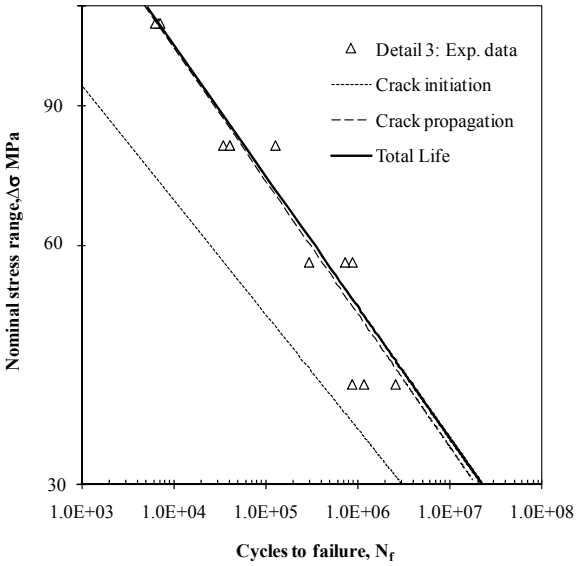

Fig. 19. Fatigue life predictions for the load-carrying fillet cruciform joint: detail 3

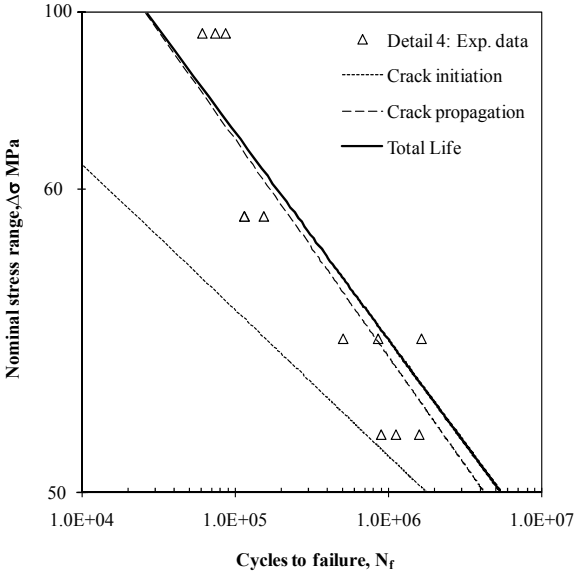

Fig. 20. Fatigue predictions for the longitudinal stiffener fillet joint: detail 4

- For the load-carrying fillet cruciform joint, the crack initiation is almost negligible, since it represents 3.5% to 6.5% of the total life for the stress ranges from 57 MPa to 114 MPa. For a stress range of 40 MPa, the importance of the crack initiation increases to about 36% of the total fatigue life.
- For the longitudinal stiffener fillet joint, crack initiation represented about 2.2% of the experimental fatigue life for the stress range of 143 MPa. The importance of the crack initiation phase increases for stress ranges between 94 and 71 MPa reaching, respectively, values of 11 to 20% of the total fatigue life.

The above comments allow the following conclusions:

- For welded joints characterized by high stress concentration factors and for high stress ranges, the initiation period is negligible. For low stress range levels, the crack initiation becomes more important.
- For welded joints characterized by low stress concentration factors, the crack initiation is meaningful, for both low and high stress ranges.

From the above discussion, it is recommended to neglect the crack initiation for the welded joints with high stress concentration factors, when loaded under high stress levels. For these cases, the crack propagation from an initial crack of 0.25 mm, leads to consistent predictions.

6. Conclusion

The fatigue life of four types of welded joints, made of 6061-T651 aluminium alloy, was predicted using a two phase model, namely to account separately for crack initiation and crack propagation phases. While the strain-life relations were used to compute the crack initiation, the LEFM was used as a base for crack propagation modelling. The required basic materials properties required for the model application were derived by means of strain-controlled fatigue tests of smooth specimens, as well as by means of fatigue crack propagation tests.

A globally satisfactory agreement between the predictions and the experimental fatigue S-N data was observed for the welded details. A 0.25 mm depth crack demonstrated to be an appropriate crack initiation criterion. The analysis of the results revealed that the crack initiation may be significant, at least for welded joints with relative lower stress concentrations and low to moderate loads. In these cases, the classical predictions based exclusively on the crack propagation, may be excessively conservative.

The proposed two-stage fatigue predicting model can be further improved in the future. Namely, residual stresses effects should be accounted at least in the local elastoplastic analysis, concerning the fatigue crack initiation prediction. The strain-life properties were only derived for the base material. However, a more accurate analysis may be performed if these properties would be derived for the welded or heat affected materials. Finally, the crack initiation criterion, which has been established on an empirical basis, requires a more fundamental definition.

7. References

ASTM (1998). ASTM E606: Standard Practice for Strain-Controlled Fatigue Testing, In: *Annual Book of ASTM Standards*, Vol. 03.01, American Society for Testing and Materials: ASTM, West Conshohocken, PA.

ASTM (2000). ASTM E647: Standard Test Method for Measurement of Fatigue Crack Growth Rates, In: *Annual Book of ASTM Standards*, Vol. 03.01, American Society for Testing and Materials: ASTM, West Conshohocken, PA.

Basquin, O.H. (1910). The Exponential Law of Endurance Tests. *ASTM*, Vol. 10, 625-630.

Borrego, L.P.; Abreu, L.M.; Costa, J.M. & Ferreira, J.M. (2004). Analysis of Low Cycle Fatigue in AlMgSi Aluminium Alloys. *Engineering Failure Analysis*, Vol. 11, 715-725.

Chung, Y.S. & Abel, A. (1988). Low Cycle Fatigue of Some Aluminum Alloys. In: *Low Cycle Fatigue*, ASTM STP 942, H. D. Solomon, G. R. Halford, L. R. Kaisand, and B. N. Leis, (Ed.), 94-106, American Society for Testing and Materials, Philadelphia, PA.

Coffin, L.F. (1954). A study of the effects of the cyclic thermal stresses on a ductile metal. *Translations of the ASME*, Vol. 76, 931-950.

De Jesus, A.M.P. (2004). *Validação de Procedimentos de Cálculo à Fadiga de Reservatórios sob Pressão*, PhD. Thesis, Universidade de Trás-os-Montes and Alto Douro, Portugal.

Maddox, S. J. (1991). *Fatigue strength of welded structures*, Second Edition, Woodhead Publishing, ISBN 978-1855730137, UK.

Manson, S.S. (1954). Behaviour of materials under conditions of thermal stress. *Technical Report No. 2933*, National Advisory Committee for Aeronautics.

Moreira, P.M.G.P.; de Jesus, A.M.P.; Ribeiro, A.S. & de Castro, P.M.S.T. (2008). Fatigue crack growth in friction stir welds of 6082-T6 and 6061-T6 aluminium alloys: A comparison. *Theoretical and Applied Fracture Mechanics*, Vol. 50, 81–91.

Morrow, J.D. (1965). Cyclic Plastic Strain Energy and Fatigue of Metals. *Int. Friction Damping and Cyclic Plasticity*, ASTM STP 378, 45-87.

Neuber, H. (1961). Theory of Stress Concentration for Shear-Strained Prismatical Bodies with Arbitrary Nonlinear Stress-Strain Law. *Translations of the ASME: Journal of Applied Mechanics*, Vol. 28, 544-550.

Paris, P.C & Erdogan, F. (1963). A critical analysis of crack propagation laws. *Journal basic Engineering Trans. ASME*, 528–534.

Radaj, D.; Sonsino, C. M. & Fricke, W. (2009). Recent developments in local concepts of fatigue assessment of welded joints. *International Journal of Fatigue*, Vol. 31, 2–11.

Ramberg, W. & Osgood, W.R. (1943). Description of stress-strain curves by three parameters, *Technical Report No. 902*, National Advisory Committee for Aeronautics.

Ribeiro, A.S. (1993). *Efeito da Fase de Iniciação na Previsão do Comportamento à Fadiga de Estruturas Soldadas*, PhD. Thesis, Universidade de Trás-os-Montes and Alto Douro, Portugal.

Ribeiro, A.S. (2001). *Estimativa da vida à fadiga de juntas soldadas. Propriedades de Resistência Mecânica da Liga de Alumínio Al 6061-T651*, Série Técnica-Científica, Ciências Aplicadas, Universidade de Trás-os-Montes e Alto Douro, ISBN 972-669-283-0, Vila Real, Portugal.

Ribeiro, A.S.; Borrego, L.P.; De Jesus, A.M.P. & Costa, J.D.M. (2009). Comparison of the low-cycle fatigue properties between the 6082-t6 and 6061-t651 aluminium alloys, *Proceedings of the 20th International Congress of Mechanical Engineering*, Gramado, RS, Brasil, November, 2009, ABCM.

Snijder, H.H. & Dijkstra, O.D. (1989). *Stress intensity factors for cracks in welded structures and containment systems*, TNO Report BI-88-128, TNO Institute for Building Materials and Structures, The Netherlands.

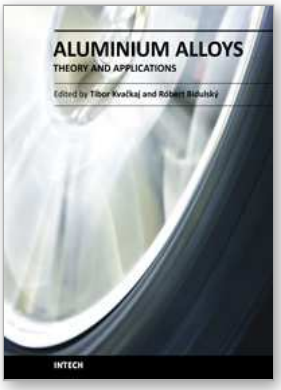

Aluminium Alloys, Theory and Applications

Edited by Prof. Tibor Kvackaj

ISBN 978-953-307-244-9
Hard cover, 400 pages
Publisher InTech
Published online 04, February, 2011
Published in print edition February, 2011

The present book enhances in detail the scope and objective of various developmental activities of the aluminium alloys. A lot of research on aluminium alloys has been performed. Currently, the research efforts are connected to the relatively new methods and processes. We hope that people new to the aluminium alloys investigation will find this book to be of assistance for the industry and university fields enabling them to keep up-to-date with the latest developments in aluminium alloys research.

How to reference

In order to correctly reference this scholarly work, feel free to copy and paste the following:

Alfredo S. Ribeiro and Abílio M.P. de Jesus (2011). Fatigue Behaviour of Welded Joints Made of 6061-T651 Aluminium Alloy, Aluminium Alloys, Theory and Applications, Prof. Tibor Kvackaj (Ed.), ISBN: 978-953-307-244-9, InTech, Available from: http://www.intechopen.com/books/aluminium-alloys-theory-and-applications/fatigue-behaviour-of-welded-joints-made-of-6061-t651-aluminium-alloy

INTECH
open science | open minds

InTech Europe
University Campus STeP Ri
Slavka Krautzeka 83/A
51000 Rijeka, Croatia
Phone: +385 (51) 770 447
Fax: +385 (51) 686 166
www.intechopen.com

InTech China
Unit 405, Office Block, Hotel Equatorial Shanghai
No.65, Yan An Road (West), Shanghai, 200040, China
中国上海市延安西路65号上海国际贵都大饭店办公楼405单元
Phone: +86-21-62489820
Fax: +86-21-62489821